DEVELOPMENT

Immotile cilia mechanically sense the direction of fluid flow for left-right determination

Takanobu A. Katoh[1,2]*, Toshihiro Omori[3]*, Katsutoshi Mizuno[1]†, Xiaorei Sai[1], Katsura Minegishi[1]‡, Yayoi Ikawa[1], Hiromi Nishimura[1], Takeshi Itabashi[4], Eriko Kajikawa[1], Sylvain Hiver[1], Atsuko H. Iwane[4], Takuji Ishikawa[3], Yasushi Okada[5,6], Takayuki Nishizaka[2], Hiroshi Hamada[1]*

Immotile cilia at the ventral node of mouse embryos are required for sensing leftward fluid flow that breaks left-right symmetry of the body. However, the flow-sensing mechanism has long remained elusive. In this work, we show that immotile cilia at the node undergo asymmetric deformation along the dorsoventral axis in response to the flow. Application of mechanical stimuli to immotile cilia by optical tweezers induced calcium ion transients and degradation of *Dand5* messenger RNA (mRNA) in the targeted cells. The Pkd2 channel protein was preferentially localized to the dorsal side of immotile cilia, and calcium ion transients were preferentially induced by mechanical stimuli directed toward the ventral side. Our results uncover the biophysical mechanism by which immotile cilia at the node sense the direction of fluid flow.

The breaking of left-right (L-R) symmetry depends on a unidirectional fluid flow at the L-R organizer in fish, amphibians, and mammals (*1*, *2*) but not in reptiles and birds (*3*, *4*). In the mouse embryo, the leftward flow at the ventral node (the L-R organizer in this species) is generated by clockwise rotation of motile cilia on pit cells located in the central region of the node. This unidirectional flow is likely sensed by immotile (primary) cilia on crown cells located at the periphery of the node (*5*). How the embryo senses this fluid flow and why the left-side cilia preferentially respond have not been understood previously. Although mechanosensing and chemosensing have each been proposed to underlie this process (*6*), the precise mechanism has remained elusive, largely as a result of technical difficulties.

Asymmetric deformation of immotile cilia in response to the flow

We first examined how immotile cilia behave in response to the nodal flow in vivo. High-speed live fluorescence imaging revealed that nodal flow induces frequent small bending movements of both left- and right-side cilia (fig. S1 and movie S1), which suggests that continuous time-independent motion, rather than bilaterally equal periodic motion, contributes to L-R symmetry breaking. To examine whether immotile cilia undergo steady-state deformation in response to nodal flow, we compared the shape of the same cilium in the presence or absence of the flow. Immotile cilia at the node were labeled with mNeonGreen with the use of NDE, a crown cell–specific enhancer derived from the mouse *Nodal* gene, whereas the cytoplasm of crown cells was labeled with tdKatushka2 (Fig. 1A). Cilia labeled with mNeonGreen were located at the periphery of the node, and most of them were negative for Foxj1 (fig. S2A). Transmission electron microscopy (TEM) also revealed that cilia at the periphery of the node lacked outer dynein arms (fig. S2C), further confirming the immotility of crown cell cilia (*5*) (movie S1). Motile cilia at the node were immobilized by ultraviolet (UV) irradiation, which is thought to induce cleavage of dynein heavy chains (*7*), and the shape of immotile cilia was observed by high-resolution microscopy before and after such irradiation (Fig. 1, B and C, and fig. S3). Nodal flow, as revealed by particle image velocimetry (PIV) analysis, was completely lost after UV irradiation for 45 s (fig. S3, A and B, and movie S2). The flow-dependent bending angle of an immotile cilium was then estimated by ellipsoidal fitting of the shape of the same cilium before and after UV irradiation (Fig. 1, D to F, and movie S3). Examination of the bending angle of immotile cilia of embryos at the two-somite stage revealed that cilia on the left side bent toward the ventral side by 5.0° ± 9.2° (mean ± SD; n = 21), whereas those on the right side bent toward the dorsal side by 4.2° ± 7.4° (n = 18) (Fig. 1, G and H). This difference in bending angle depended on the presence of the leftward flow, given that it was lost in *iv/iv* mutant embryos (Fig. 1H), which lack nodal flow, and it was dependent on embryonic stage (Fig. 1H). The bending angle was thus significantly asymmetric along the dorsoventral (D-V) axis at the two- and three-somite stages, when the velocity of nodal flow is maximal, whereas it did not manifest asymmetry at the late headfold (LHF) and zero-somite stages, when the flow is absent or weak, respectively (*8*) (Fig. 1H). This asymmetric bending of immotile cilia along the D-V axis is consistent with the direction of the flow. Modeling the flow on the basis of in vivo observations thus suggested the presence of a ventrally directed flow at the left-posterior region of the node and a dorsally directed flow on the right side of the node (fig. S4 and movie S4). There was no significant asymmetry in the bending angle along the anterior-posterior (A-P) axis of embryos examined between the LHF and three-somite stages (fig. S3F). Notably, immotile cilia with the largest extent of ventral bending were preferentially observed at the left-posterior region of the node (Fig. 1G and fig. S3E), where the ventrally directed flow is prominent (fig. S4C) and the first molecular asymmetry appears (*9*).

Immotile cilia at the node respond to mechanical stimuli

Given that immotile cilia on the right and left sides of the node were found to bend asymmetrically along the D-V axis in response to the leftward fluid flow, we next tested whether immotile cilia at the node respond to mechanical force with the use of optical tweezers (*10*, *11*) (Fig. 1B and fig. S5). We examined mouse embryos harboring two transgenes (Fig. 2, A and B, and movie S5)—one to visualize perinodal immotile cilia and the other to monitor the response to mechanical stimuli. *Dand5* mRNA is the ultimate target of nodal flow (*12*, *13*), being degraded by the Bicc1-Ccr4 complex in response to the flow (*14*). Crown cells were labeled with the *NDE4-hsp-dsVenus-Dand5-3′-UTR* transgene, with the level of dsVenus mRNA reflecting that of *Dand5* mRNA (*14*), whereas their immotile cilia were visualized with a transgene encoding mCherry. We applied whole-cell fluorescence recovery after photobleaching (FRAP) to examine the kinetics of *Dand5* mRNA after subjecting an immotile cilium to mechanical stimuli (fig. S6A). We first tested the validity of the whole-cell FRAP system. According to a theoretical model, the rate of fluorescence recovery depends on the mRNA level (fig. S6B). In wild-type embryos with a leftward flow, the level of fluorescence on the right side of the node rapidly recovered after photobleaching, consistent with the predicted FRAP curve, whereas the level of recovery was much lower on the left side (fig. S6C). These observations confirmed that the whole-cell FRAP system was able to monitor the kinetics of *Dand5* mRNA.

[1]Laboratory for Organismal Patterning, RIKEN Center for Biosystems Dynamics Research, Kobe, Hyogo, Japan. [2]Department of Physics, Faculty of Science, Gakushuin University, Toshima-ku, Tokyo, Japan. [3]Graduate School of Biomedical Engineering, Tohoku University, Aoba Aramaki, Sendai, Miyagi, Japan. [4]RIKEN Center for Biosystems Dynamics Research, Higashi-Hiroshima, Hiroshima, Japan. [5]Laboratory for Cell Polarity Regulation, RIKEN Center for Biosystems Dynamics Research, Suita, Osaka, Japan. [6]Department of Cell Biology and Physics, Universal Biology Institute and International Research Center for Neurointelligence, The University of Tokyo, Hongo, Tokyo, Japan.
*Corresponding author. Email: takanobu.a.katoh@gmail.com (T.A.K.); omori@tohoku.ac.jp (T.O.); hiroshi.hamada@riken.jp (H.H.)
†Present address: Department of Cell Biology and Biochemistry, Division of Medicine, Faculty of Medical Sciences, University of Fukui, Eiheiji-cho, Yoshida-gun, Fukui, Japan.
‡Present address: Department of Molecular Therapy, National Institutes of Neuroscience, National Center of Neurology and Psychiatry, Kodaira, Tokyo, Japan.

Mechanical stimuli were administered under a condition that mimics nodal flow to individual immotile cilia of *iv/iv* embryos (which lack nodal flow) at the early headfold (EHF) stage to the three-somite stage by positioning a polystyrene bead (with a diameter of 3.5 μm) trapped by optical tweezers into contact with the cilium and displacing it 1.75 μm toward the ventral side and then 1.75 μm toward the dorsal side at a frequency of 2 Hz (Fig. 2C and movie S6). The amplitude is within the physiological range (fig. S3G), and the maximal trapping force of ~±12 pN was sufficient to apply mechanical bending to an immotile cilium (fig. S5A). Observation of beads by three-dimensional (3D) single-particle tracking microscopy (*15*, *16*) confirmed that they moved along the D-V axis (fig. S5C). The infrared laser of the optical tweezers did not exert any unexpected effects, such as a change in Ca^{2+} oscillation pattern in crown cells or cilia (fig. S7 and materials and methods). After administration of mechanical stimuli to an immotile cilium for 1.5 hours, all crown cells were subjected twice to uniform photobleaching with a recovery period of 30 min after each bleaching. The timing and duration of the stimulation matched our previous in vivo observations (*8*). The recovery of dsVenus fluorescence in the cell with the stimulated cilium and in neighboring unstimulated ciliated cells was monitored by time-lapse 3D imaging (Fig. 2, D and E; fig. S6D; and movie S7). The fluorescence intensity at 30 min after each bleaching had reached a plateau and was compared between stimulated and neighboring cells (Fig. 2F and fig. S6E). The extent of fluorescence recovery in the stimulated cell was substantially lower than that in the unstimulated cells, with values of 69.9 ± 21.5% at 2 hours and 53.0 ± 20.9% at 2.5 hours after the onset of stimulation (geometric means ± SDs; n = 28) (Fig. 2G), which suggests that mechanical stimulation of an immotile cilium was able to induce degradation of *Dand5* mRNA. Immotile cilia on the right and left sides of the node of *iv/iv* embryos responded similarly to the mechanical stimuli (Fig. 2H). Those on the right side of the node of wild-type embryos (in the presence of the endogenous nodal flow) also showed a similar response to mechanical stimuli (Fig. 2I; fig. S6, G to I; and movie S8). Administration of mechanical stimuli to the cell body of a crown cell instead of to its cilium did not affect recovery of the fluorescence signal (Fig. 2G). Furthermore, the response to mechanical stimuli was lost in embryos lacking the cation channel Pkd2 (Fig. 2I), which suggests that mechanical stimulation of immotile cilia induces degradation of *Dand5* mRNA in a Pkd2-dependent manner. Mechanical stimulation for 45 min instead of 1.5 hours was sufficient to promote *Dand5* mRNA degradation (fig. S6J).

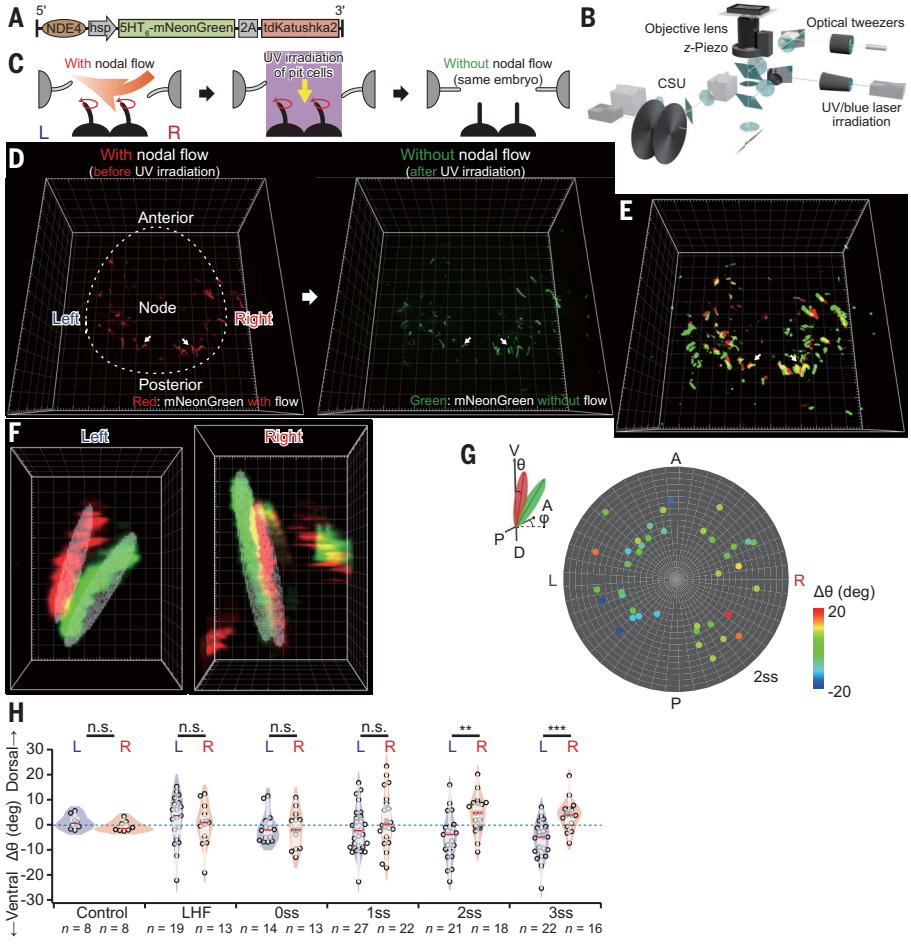

Fig. 1. Immotile cilia at the node of mouse embryos undergo asymmetric deformation along the D-V axis in response to nodal flow. (**A**) Schematic of the transgene. Immotile cilia at the node are visualized on the basis of mNeonGreen expression that is under the control of the NDE and is targeted to cilia by a 5-hydroxytryptamine receptor isoform 6 ($5HT_6$) sequence. (**B**) Schematic of the optical pathway for analysis. A UV laser and blue laser for irradiation are introduced into a microscope, which is equipped with a spinning-disk confocal unit (CSU) and optical tweezers. (**C**) Schematic of the experiment. Live fluorescence images of immotile cilia at the node were first obtained in the presence of nodal flow. The central region of the node encompassing pit cells was then subjected to UV irradiation to abolish nodal flow, and fluorescence images of immotile cilia in the absence of the flow were obtained from the same embryo. (**D**) High-resolution 3D images obtained by deconvolution processing of immotile cilia (fig. S3D) in the presence (left) or absence (right) of nodal flow. Cilia shown in red or green correspond to those in the presence or absence of the flow, respectively. Grid size, 10 μm. (**E**) Detection of the edge of each cilium after alignment. Immotile cilia of the same embryo are shown in the presence (red) and absence (green) of the flow. Grid size, 10 μm. (**F**) Individual immotile cilia on the left or right side of the node in the presence (red) or absence (green) of the flow. The zenith and azimuth angles were determined by ellipsoidal fitting (gray mesh) of the edge of each cilium. Grid size, 1 μm. (**G**) Distribution of immotile cilia at the node with various values of Δθ (change in the zenith angle in response to the flow). Data were obtained from wild-type embryos (n = 39 cilia from 7 embryos) at the two-somite (2ss) stage (fig. S3E). A, anterior; P, posterior; R, right; L, left; V, ventral; D, dorsal. (**H**) Δθ values [degrees (deg)] for immotile cilia on the left and right sides of the node were determined at various developmental stages. Data for *iv/iv* embryos at the LHF stage to the 2ss stage are shown as a control. Red bars indicate median values. $^{**}P < 0.01$; $^{***}P < 0.001$; n.s., not significant (Mann-Whitney U test).

The response to mechanical stimuli was further confirmed with another readout: expression of the transgene *ANE-LacZ*, which allows monitoring of Nodal activity in perinodal cells (*17*). This transgene manifests left-sided expression at the node in the presence of nodal flow but shows L-R randomized expression in its absence (*9*) (fig. S6F). Mechanical stimulation along the D-V axis of an immotile cilium on the right side of an *iv/iv* embryo resulted in a significant increase in the R/(R + L) ratio of *ANE-LacZ* expression to 0.64 ± 0.19 (mean ± SD; n = 12) compared with a value of 0.47 ± 0.22 (n = 24) for control embryos (Fig. 2J). These

results suggested that mechanical stimulation of a single immotile cilium not only induced degradation of *Dand5* mRNA in the targeted cell but also established molecular asymmetry in all crown cells at the node. A feedback mechanism involving Wnt and Dand5 signals (*12*) may be responsible for the expansion of asymmetric Nodal activity among crown cells.

Perinodal cells of mouse embryos manifest both cytoplasmic and intraciliary Ca^{2+} transients in response to nodal flow (*18*–*20*). We therefore examined whether mechanical stimuli administered to immotile cilia of *iv/iv* embryos might induce such transients. Cytoplasmic and intraciliary Ca^{2+} transients were observed with cytoplasm-targeted and cilium-targeted (*18*) forms of the fluorescent Ca^{2+} indicator GCaMP6, respectively (Fig. 3, A and B). Spontaneous Ca^{2+} transients were detected in both the cytoplasm and immotile cilia (Fig. 3C), with such transients having been shown to be independent of nodal flow and the Pkd2 channel (*18*, *19*). However, the frequency of Ca^{2+} transients increased significantly from 0.83 ± 0.71 to 1.39 ± 1.65 spikes per minute in the cytoplasm (means ± SDs; n = 42 cells) and from 0.32 ± 0.57 to 0.59 ± 1.02 spikes per minute in cilia (n = 24) in response to mechanical stimuli (Fig. 3, C and D, and movie S9). Such increases in the frequency of cytoplasmic and ciliary Ca^{2+} transients were not observed in embryos lacking the Pkd2 channel (Fig. 3E).

Immotile cilia sense bending direction in a manner dependent on polarized localization of Pkd2

We next investigated whether an immotile cilium might respond differentially to forced bending toward the dorsal or ventral sides, possibly as a result of a structure or molecule within the cilium that can sense the direction of bending. The polarized distribution of such a structure or molecule relative to the midline of an embryo would allow a differential response to the direction of nodal flow (fig. S8A). We first searched for such a structure at or near the base of immotile cilia by focused ion beam–scanning electron microscopy (FIB-SEM), which would be expected to reveal an

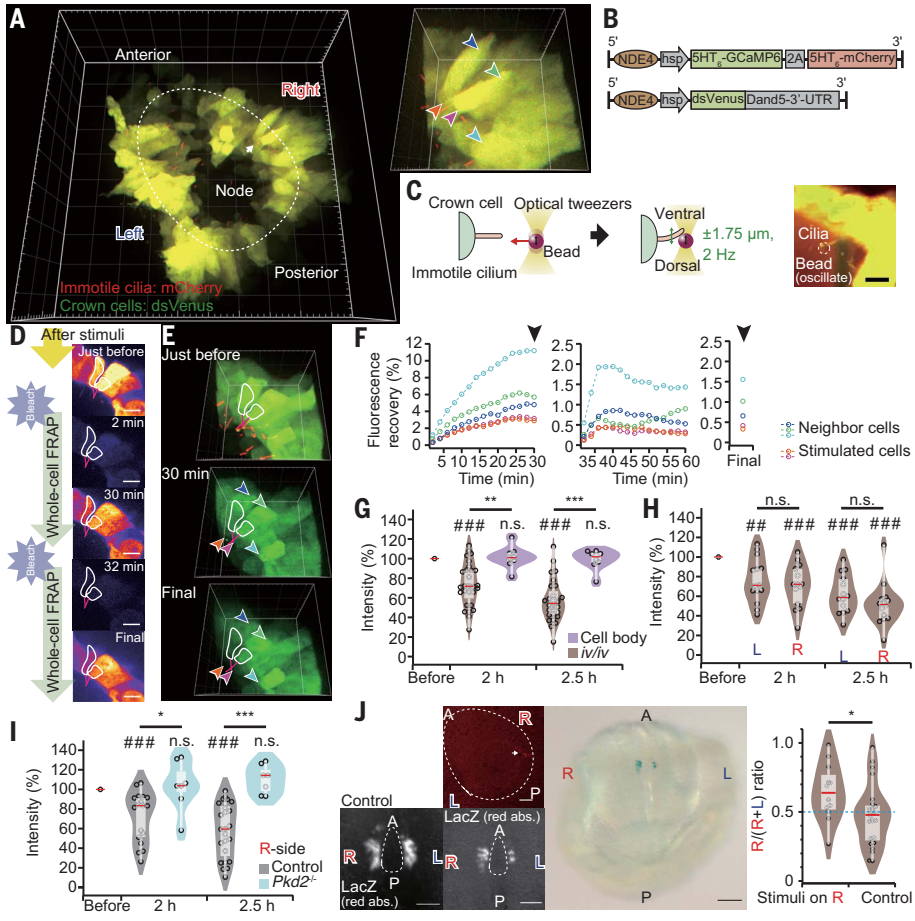

Fig. 2. Mechanical stimuli administered to immotile cilia by optical tweezers trigger *Dand5* mRNA degradation and increase Nodal activity. (**A**) A 3D image of the node of an *iv/iv* mouse embryo at the two-somite stage harboring the two transgenes shown in (B). mCherry (red) marks immotile cilia, whereas *Dand5* mRNA degradation in crown cells can be monitored by measurement of dsVenus fluorescence (green). The white arrow indicates cilia to which mechanical stimuli were applied. Grid size, 20 μm. The cells to which mechanical stimuli were applied (orange and purple arrowheads) and surrounding unstimulated cells (blue, green, and cyan arrowheads) are also shown at higher magnification to the right of the main image. Grid size, 10 μm. (**B**) Schematic of the two transgenes adopted for these experiments. UTR, untranslated region. (**C**) Experimental scheme. A polystyrene bead is trapped, placed into contact with an immotile cilium, and forced to oscillate along the D-V axis for 1.5 hours with the use of optical tweezers. The image on the right shows an oscillating bead (white dotted line) making contact with cilia (movie S6). (D to H) Analysis of *iv/iv* embryos at the EHF to three-somite stages. (**D**) *Dand5* mRNA degradation was monitored by whole-cell FRAP (fig. S6, A to C). The entire area of the targeted cells was bleached twice with a 30-min interval between sessions, and fluorescence recovery was monitored. White dotted lines indicate the stimulated cells. 2D sections obtained from 3D images are shown. Scale bars, 10 μm. (**E**) 3D images obtained during FRAP. Red, purple, blue, green, and cyan arrowheads represent the same cells shown in (A). Grid size, 10 μm. (**F**) Time course of fluorescence recovery during the first and second FRAP periods. A 3D image was obtained with a longer exposure time at the end of the second FRAP session (fig. S6E). Normalized intensity was calculated with the use of the values indicated by the closed arrowheads and is shown in (G). (**G**) Normalized fluorescence intensity of dsVenus is shown for before as well as 2 and 2.5 hours after stimulation (brown; n = 28 embryos). Data are also shown for cells whose cell body (instead of the cilium) was stimulated (purple; n = 8 embryos). Red bars indicate median values. (**H**) Normalized fluorescence intensity of dsVenus before and after stimulation for immotile cilia on the left and right sides (n = 14 embryos each for left-side cilia and right-side cilia). (**I**) Normalized fluorescence intensity of dsVenus for similar FRAP experiments performed with *Pkd2*$^{-/-}$ and control (wild-type, *iv/+*, or *Pkd2*$^{+/-}$) embryos (n = 7 for *Pkd2*$^{-/-}$ and 22 for control embryos). The experiments were performed only with immotile cilia on the right side to avoid the effect of nodal flow. (**J**) A single cilium on the right side of an *iv/iv* embryo harboring the *ANE-LacZ* transgene was subjected to mechanical stimulation for 1.5 hours (arrow in the mCherry fluorescence image shown in the upper left), cultured for ~7 hours, and then subjected to X-gal staining to detect Nodal activity (large middle panel) (fig. S6F). The level of staining was quantified as red absorbance (lower left), and the ratio of the staining level on the right side to that on the right plus left sides of the node [R/(R + L)] was determined (right) for embryos subjected to mechanical stimulation or nonstimulated (control) embryos. Scale bars, 20 μm (upper left), 50 μm (lower left), and 100 μm (middle). ##P < 0.01; ###P < 0.001 [Wilcoxon signed-rank test for comparisons of before with 2 and 2.5 hours in (G) to (I)]. *P < 0.05; **P < 0.01; ***P < 0.001 [Mann-Whitney U test in (G) to (J)].

anisotropic distribution relative to the midline, but we were not successful (fig. S8B). Consistent with this result, measurement of the flexural rigidity of immotile cilia with optical tweezers revealed no apparent difference between dorsal and ventral bending (fig. S9).

Alternatively, a mechanosensitive channel may be preferentially localized to one side (dorsal or ventral) of an immotile cilium. The most likely candidate for such a channel would be Pkd2, given that the ciliary localization of this protein is essential for the breaking of L-R symmetry (*5*, *21*). We examined the precise localization of Pkd2 within immotile cilia by 3D stimulated emission depletion (STED) microscopy of wild-type embryos harboring an *NDE2-hsp-Pkd2-Venus* transgene, which is able to rescue the defects of Pkd2-deficient mouse embryos (*5*). The super-resolution images revealed a nonuniform distribution of the Pkd2::Venus protein on each immotile cilium. The Pkd2::Venus protein thus accumulated to form clusters on the surfaces of immotile cilia, with the clusters being preferentially localized to the dorsal side (the side facing the midline of the embryo) of those on both the left and right sides of the embryo (Fig. 4A and movie S10). Analysis of the angular distribution of Pkd2::Venus on the transverse plane of the axoneme revealed that the D/(D + V) ratio of Pkd2 signal intensity was significantly biased toward the dorsal side (0.54 ± 0.12, mean ± SD; n = 50) (Fig. 4B). Preferential localization of Pkd2 on the dorsal side of immotile cilia was confirmed by confocal microscopy with the Airyscan detector. Analysis of the distance along the z axis between the center of localization of Pkd2 and that of the axoneme by Gaussian fitting revealed that the Pkd2 region was displaced toward the dorsal side by 142 ± 92 nm in cilia on the left side (mean ± SD; n = 53) and by 192 ± 203 nm in those on the right side (n = 54) (Fig. 4C; fig. S10, A to C; and movie S11), with these distances being compatible with a value of 100 nm for the radius of an axoneme. Furthermore, images of longitudinal sections of immotile cilia also confirmed the dorsal localization of Pkd2 (fig. S10E). By contrast, there was no significant enrichment of Pkd2 along the proximodistal axis of a cilium (fig. S10D). Endogenous Pkd2 also showed a similar preferential distribution to the dorsal side of immotile cilia as examined with the use of antibodies to Pkd2 (fig. S11).

Enrichment of Pkd2 at the dorsal side of a cilium could explain how immotile cilia sense the direction of nodal flow (Fig. 4D). Imposition of mechanical stimuli in a single direction and measurement of cytoplasmic Ca^{2+} transients revealed that immotile cilia showed a significantly greater response to stimuli directed toward the ventral side than to those directed toward the dorsal side (Fig. 4E, fig. S12, and movie S12). Dorsal bending generated a greater response than ventral bending regardless of the order of bending direction (fig. S12, C and D). Examination of the Pkd2 expression pattern by generation of *Pkd2*^{mNG} mice, in which the amino acid sequence for mNeonGreen was knocked in at the COOH-terminus of Pkd2, revealed that the Pkd2::mNeonGreen protein was present mostly in immotile cilia of crown cells (fig. S2B).

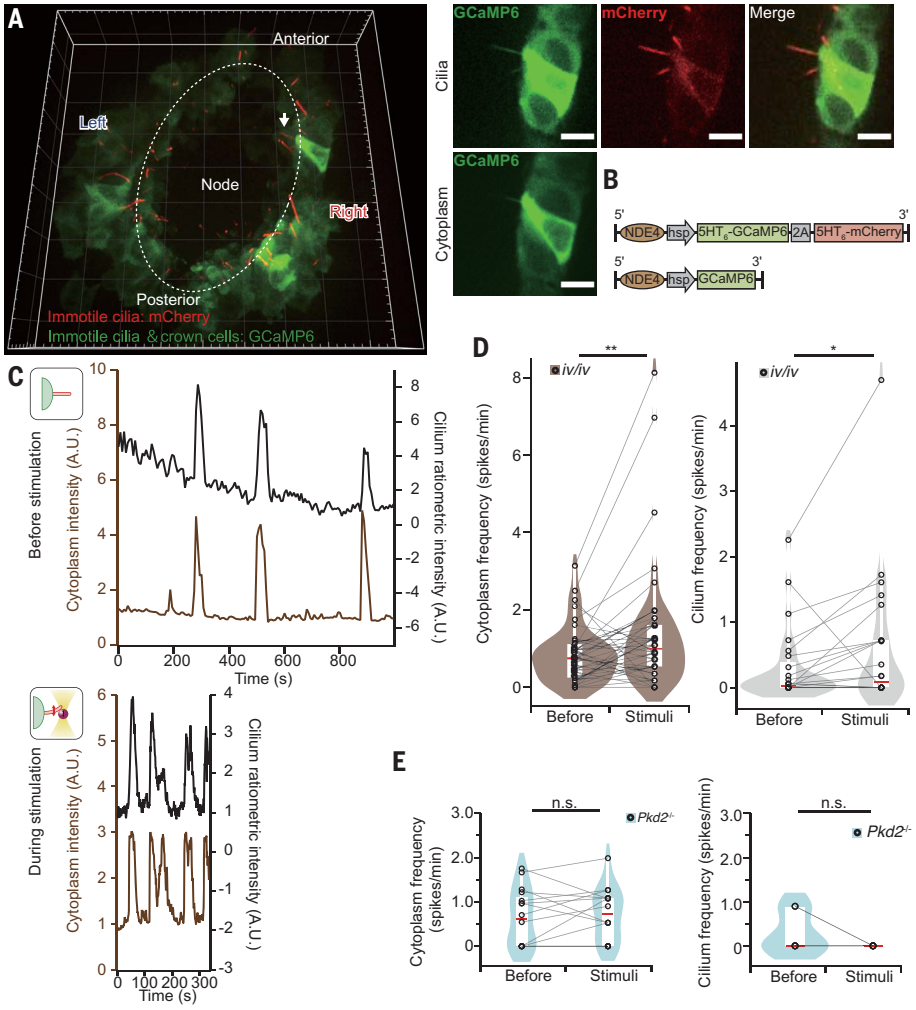

Fig. 3. Mechanical stimulation of the immotile cilium of crown cells alters the dynamics of Ca^{2+} signaling in both the cilium and cytoplasm. (**A**) A 3D image of the node of an *iv/iv* embryo at the two-somite stage harboring the two transgenes in (B) is shown on the left. The white arrow indicates a cilium to which mechanical stimuli were applied. Grid size, 10 μm. Both GCaMP6 and mCherry are expressed in immotile cilia for ratiometric Ca^{2+} imaging, with sections containing the cilium being averaged (upper right). GCaMP6 is also expressed in the cytoplasm for cytoplasmic Ca^{2+} imaging, with sections containing the cell body being averaged (lower right). Scale bars, 10 μm. (**B**) Schematic of the two transgenes used for intracellular Ca^{2+} measurement. (**C**) Time course of Ca^{2+} signal intensity before (top) and during (bottom) stimulation of the immotile cilium of a crown cell in an *iv/iv* embryo. Brown traces indicate cytoplasmic Ca^{2+} (GCaMP6 F/F_0 ratiometric values), whereas black traces indicate intraciliary Ca^{2+} (GCaMP6/mCherry F/F_0 ratiometric values). Calcium dynamics in the cilium and cytoplasm were monitored for ~15 min before (upper) and then for ~5 min after (lower) the onset of mechanical stimulation of the cilium (movie S9). A.U., arbitrary units. (**D**) The mean frequency of Ca^{2+} transients in the cytoplasm (left) and cilium (right) was measured as in (C) (n = 42 cells from 28 embryos for cytoplasm and 24 cilia from 17 embryos for cilia). (**E**) Mean frequency of Ca^{2+} transients in the cytoplasm and cilium of *Pkd2*$^{-/-}$ embryos (n = 16 cells from 16 embryos for cytoplasm and 6 cilia from 6 embryos for cilia). *P < 0.05; **P < 0.01 [Wilcoxon signed-rank test in (D) and (E)].

Discussion

Our results collectively indicate that immotile cilia at the node respond to mechanical force generated by fluid flow. This notion contradicts the previous claim that primary cilia do not function as Ca^{2+}-dependent mechanosensors (*22*) but is supported by similar findings with zebrafish embryos in an accompanying paper (*23*). Given that the relative extent of viscous

and bending force is approximately given by length^4/stiffness$^{0.25}$ (*24*), the slender shape of a cilium is suited to sensing a weak flow and transducing the flow signal into strong locoregional strain. In the presence of leftward flow, the bending of an immotile cilium on the left side of the node toward the ventral side imposes a strain of 0.014 ± 0.013 (mean ± SD; n = 8) to the dorsal side of the cilium (Fig. 4, F and G). The resulting membrane tension, according to a previously described model (*25*), would be 1.6 ± 1.6 mN/m (mean ± SD; n = 8) (fig. S13), which may be sufficient to activate dorsally localized Pkd2 and trigger the Ca^{2+} response. By contrast, on the right side of the node, strain at the dorsal side of an immotile cilium is as small as 0.000 ± 0.001 (n = 8) and would not support a response (Fig. 4, F and G).

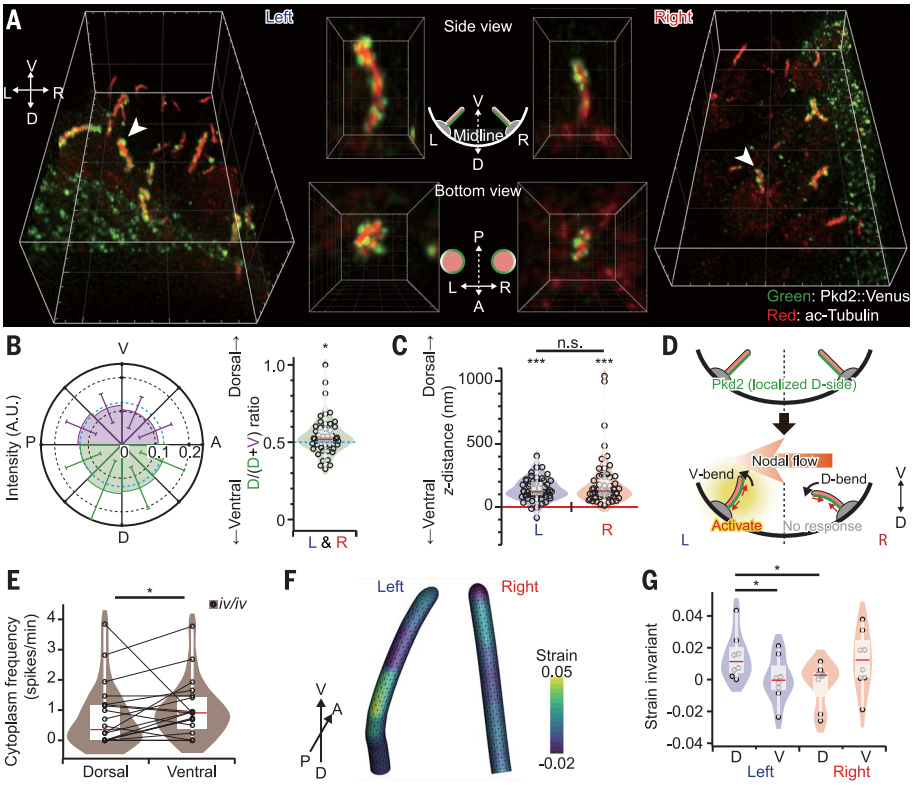

Fig. 4. Immotile cilia sense bending direction in a manner dependent on polarized localization of Pkd2. (**A**) A wild-type mouse embryo harboring an *NDE2-hsp-Pkd2-Venus* transgene was subjected to immunofluorescence analysis for detection of the Pkd2::Venus fusion protein and acetylated (ac)–tubulin at the node with a 3D-STED microscope (left and right images). Magnified views of D-V sections and bottom views of cilia (indicated by white arrowheads in left and right images) shown in the middle suggest a preferential localization of Pkd2::Venus at the dorsal side of cilia on both the left and right sides of the node. Grid size, 5 μm (main panels), 1 μm (side views), and 0.5 μm (bottom views). (**B**) The angular distribution of green fluorescence intensity in transverse planes of each cilium imaged as in (A) was analyzed (left). The ratio of Pkd2::Venus signal intensity on the dorsal side to that on the dorsal plus ventral sides [D/(D + V)] (right) was significantly biased toward the dorsal side (n = 50 cilia from 4 embryos). *P < 0.05 (one-sample t test). (**C**) Distance along the z axis between the centers of red and green fluorescence intensity in longitudinal optical sections of each cilium obtained by an Airyscan microscope (fig. S10B) was measured by Gaussian fitting after precise correction for chromatic aberration. The intensity center for Pkd2::Venus was significantly polarized toward the dorsal side of cilia on both the left and right sides (n = 53 cilia for the left side and 54 cilia for the right side from 13 embryos). ***P < 0.001 (one-sample t test). Wilcoxon signed-rank test was used for comparison of left and right sides. (**D**) Model that would explain why immotile cilia on the left side, but not those on the right side, respond to the leftward fluid flow. (**E**) Frequency of cytoplasmic Ca^{2+} transients in individual immotile cilia subjected to both dorsal and ventral bending (n = 18 cilia from 18 *iv/iv* embryos) (fig. S12, A and B). Whereas the frequency was 0.81 ± 1.03 spikes per minute (mean ± SD) for dorsal bending, it was significantly increased to 1.02 ± 0.93 spikes per minute for ventral bending. *P < 0.05 (Wilcoxon signed-rank test). (**F**) Estimated strain at the membrane of the immotile cilia on the left and right sides of the node shown in Fig. 1F. The membrane is modeled as a 2D hyperelastic material, and the contour color indicates the second strain invariant. (**G**) Comparison of strain applied to the dorsal and ventral sides of cilia on the left or right sides of the node. The mean value of the second strain invariant was used as the basis for strain measurement. Definition of the dorsal and ventral regions is described in fig. S13B. Strains on the dorsal and ventral sides of a left-side cilium are estimated as 0.014 ± 0.013 and 0.000 ± 0.013 (means ± SDs; n = 8), respectively, whereas the corresponding values for a right-side cilium are 0.000 ± 0.001 and 0.012 ± 0.017 (n = 8), respectively. *P < 0.05 (Student's paired t test).

Our findings thus suggest how immotile cilia sense the direction of nodal flow: Directional information of the flow is geometrically converted to locoregional strain, which is integrated over the polarized area of Pkd2 localization and allows activation only of cilia on the left side, thereby giving rise to robust L-R determination. Given that other proteins, such as the channel protein Hv1 (*26*) and the structural protein LRRCC1 (*27*), show asymmetric localization within cilia and the centriole, respectively, additional molecules may be localized asymmetrically in immotile cilia at the node and render the mechanism responsible for the breaking of L-R symmetry more robust.

Several questions remain, including how Pkd2 becomes preferentially localized to one side of an immotile cilium. Crown cells on the left and right sides of the node may be polarized relative to the midline, given that the organization of centrioles in crown cells on both sides was found to be polarized along the mediolateral axis (fig. S14). An unknown signal derived from the midline of the embryo may polarize Pkd2 localization. Bone morphogenetic protein (BMP) antagonists expressed at the node are candidates for such a signal. However, treatment of embryos with exogenous BMP did not affect the localization of Pkd2 at the dorsal side of immotile cilia (fig. S10F). Characterization of the mechanism responsible for the polarized localization of Pkd2 therefore awaits further study.

REFERENCES AND NOTES

1. M. Blum, K. Feistel, T. Thumberger, A. Schweickert, *Development* **141**, 1603–1613 (2014).
2. H. Shiratori, H. Hamada, *Development* **133**, 2095–2104 (2006).
3. J. Gros, K. Feistel, C. Viebahn, M. Blum, C. J. Tabin, *Science* **324**, 941–944 (2009).
4. E. Kajikawa *et al.*, *Nat. Ecol. Evol.* **4**, 261–269 (2020).
5. S. Yoshiba *et al.*, *Science* **338**, 226–231 (2012).
6. J. H. E. Cartwright, O. Piro, I. Tuval, *Phil. Trans. R. Soc. B* **375**, 20190566 (2020).
7. B. H. Gibbons, I. R. Gibbons, *J. Biol. Chem.* **262**, 8354–8359 (1987).
8. K. Shinohara *et al.*, *Nat. Commun.* **3**, 622 (2012).
9. A. Kawasumi *et al.*, *Dev. Biol.* **353**, 321–330 (2011).
10. A. Ashkin, *Proc. Natl. Acad. Sci. U.S.A.* **94**, 4853–4860 (1997).
11. T. A. Katoh *et al.*, *Sci. Rep.* **8**, 15562 (2018).
12. T. Nakamura *et al.*, *Nat. Commun.* **3**, 1322 (2012).
13. A. Schweickert *et al.*, *Curr. Biol.* **20**, 738–743 (2010).
14. K. Minegishi *et al.*, *Nat. Commun.* **12**, 4071 (2021).
15. H. P. Kao, A. S. Verkman, *Biophys. J.* **67**, 1291–1300 (1994).
16. B. Huang, W. Wang, M. Bates, X. Zhuang, *Science* **319**, 810–813 (2008).
17. K. Yashiro *et al.*, *Genes Cells* **5**, 343–357 (2000).
18. K. Mizuno *et al.*, *Sci. Adv.* **6**, eaba1195 (2020).
19. D. Takao *et al.*, *Dev. Biol.* **376**, 23–30 (2013).
20. J. McGrath, S. Somlo, S. Makova, X. Tian, M. Brueckner, *Cell* **114**, 61–73 (2003).

21. S. Field *et al*., *Development* **138**, 1131–1142 (2011).
22. M. Delling *et al*., *Nature* **531**, 656–660 (2016).
23. L. Djenoune *et al*., *Science* **379**, 71–78 (2023).
24. M. C. Lagomarsino, F. Capuani, C. P. Lowe, *J. Theor. Biol.* **224**, 215–224 (2003).
25. R. Skalak, A. Tozeren, R. P. Zarda, S. Chien, *Biophys. J.* **13**, 245–264 (1973).
26. M. R. Miller *et al*., *Cell Rep.* **24**, 2606–2613 (2018).
27. N. Gaudin *et al*., *eLife* **11**, e72382 (2022).

ACKNOWLEDGMENTS

We thank Y. Kiyosue for support with microscopy systems; K. Kawaguchi and members of his laboratory as well as S. Nonaka for discussions; D. Takao for support with STED imaging; Tokai Electron Microscopy, Inc., for TEM imaging; the Laboratory for Ultrastructural Research (RIKEN BDR) for technical support; the Laboratory for Animal Resource and Genetic Engineering (RIKEN, BDR) for generating the *Pkd2*^{mNG} knock-in mouse; K. Takaoka, T. Ide, H. M. Takase, and K. Shiozawa for technical advice; and T. Lange for technical assistance. **Funding:** This study was supported by grants from the Ministry of Education, Culture, Sports, Science, and Technology (MEXT) of Japan (no. 17H01435) and from Core Research for Evolutional Science and Technology (CREST) of the Japan Science and Technology Agency (JST) (no. JPMJCR13W5) to H.H.; by a Grant-in-Aid (no. 21K15096) from the Japan Society for the Promotion of Science (JSPS) and by the RIKEN Special Postdoctoral Researcher Program to T.A.K.; by a grant from Precursory Research for Embryonic Science and Technology (PRESTO) of JST (no. JPMJPR2142) to T.O.; by grants from JSPS (nos. 21H04999 and 21H05308) to T.I.; and by RIKEN Cluster for Science, Technology, and Innovation Hub (RCSTI) to A.H.I. 3D-STED microscopy was supported by grants from JST (nos. JPMJMS2025-15, JPMJCR20E2, JPMJCR15G2, and JPMJCR1852) and from JSPS (nos. 19H05794 and 16H06280) to Y.O. **Author contributions:** T.A.K. and T.N. designed experiments with optical tweezers. T.A.K. performed biophysical experiments with mouse embryos and analyzed the data. T.O. and T.Is. are responsible for theoretical analysis of immotile cilia. Y.I. and H.N. generated transgenic mice. S.H. genotyped transgenic mice. K.Miz. helped with analysis of Ca^{2+} transients and highly inclined and laminated optical sheet (HILO) imaging. K.Min. helped with analysis of *Dand5* mRNA degradation. E.K. examined ANE-LacZ activity. X.S. performed immunostaining. T.It. and A.H.I. performed FIB-SEM analysis of immotile cilia. Y.O. assisted with STED analysis. T.A.K., T.O., and H.H. conceived the project and wrote the paper. **Competing interests:** The authors declare no competing interests. **Data and materials availability:** All data are available in the manuscript or the supplementary materials.

SUPPLEMENTARY MATERIALS

science.org/doi/10.1126/science.abq8148
Materials and Methods
Figs. S1 to S14
References (*28*–*46*)
MDAR Reproducibility Checklist
Movies S1 to S12

View/request a protocol for this paper from *Bio-protocol*.

Submitted 2 May 2022; resubmitted 1 November 2022
Accepted 9 December 2022
10.1126/science.abq8148

Immotile cilia mechanically sense the direction of fluid flow for left-right determination

Takanobu A. KatohToshihiro OmoriKatsutoshi MizunoXiaorei SaiKatsura MinegishiYayoi IkawaHiromi NishimuraTakeshi ItabashiEriko KajikawaSylvain HiverAtsuko H. IwaneTakuji IshikawaYasushi OkadaTakayuki NishizakaHiroshi Hamada

Science, 379 (6627), • DOI: 10.1126/science.abq8148

Going with the flow

In most vertebrates, left-right differences are specified during early embryogenesis by a small cluster of cells called the left-right organizer. Within this organizer, motile cilia move rapidly to create a leftward directional flow of extracellular fluid that is the first sign of a left-right difference, but how this flow is sensed and transduced into later molecular and anatomical left-right asymmetry has been unclear. Working with mouse embryos, Katoh *et al*. found that immotile cilia sense the mechanical force generated by the flow and suggest a biophysical mechanism by which the direction of the flow is sensed. Independently, working in zebrafish, Djenoune *et al*. used optical tweezers and live imaging to show that immotile cilia in the organizer function as mechanosensors that translate extracellular fluid flow into calcium signals. When motile cilia were paralyzed and normal flow stopped, mechanical manipulation of the cilia could rescue, or even reverse, left-right patterning. Thus, ciliary force sensing is necessary, sufficient, and instructive for embryonic laterality. —SMH